

ON ACCELERATED ITERATIVE SCHEMES FOR ANISOTROPIC RADIATIVE TRANSFER USING RESIDUAL MINIMIZATION

RICCARDO BARDIN ^{*} AND MATTHIAS SCHLOTTBOM [†]

Abstract. We consider the iterative solution of anisotropic radiative transfer problems using residual minimization over suitable subspaces. We show convergence of the resulting iteration using Hilbert space norms, which allows us to obtain algorithms that are robust with respect to finite-dimensional realizations via Galerkin projections. We investigate in particular the behavior of the iterative scheme for discontinuous Galerkin discretizations in the angular variable in combination with subspaces that are derived from related diffusion problems. The performance of the resulting schemes is investigated in numerical examples for highly anisotropic scattering problems with heterogeneous parameters.

Key words. anisotropic radiative transfer, iterative solution, nonlinear preconditioning, convergence

AMS subject classifications. 65F08, 65F10, 65N22, 65N30, 65N45

1. Introduction. The radiative transfer equation serves as a fundamental tool in predicting the interaction of electromagnetic radiation with matter, modeling scattering, absorption and emission. As such, it has a key role in many scientific and societal applications, including medical imaging and tumor treatment [3, 16], energy efficient generation of white light [26], climate sciences [14, 30], geosciences [20], and astrophysics [25]. The stationary monochromatic radiative transfer equation is an integro-differential equation of the form

$$(1.1) \quad \mathbf{s} \cdot \nabla u(\mathbf{r}, \mathbf{s}) + \sigma_t(\mathbf{r})u(\mathbf{r}, \mathbf{s}) = \sigma_s(\mathbf{r}) \int_{S^{d-1}} \theta(\mathbf{s} \cdot \mathbf{s}')u(\mathbf{r}, \mathbf{s}') d\mathbf{s}' + q(\mathbf{r}, \mathbf{s}) \quad \text{for } (\mathbf{r}, \mathbf{s}) \in D := R \times S^{d-1},$$

where the specific intensity $u = u(\mathbf{r}, \mathbf{s})$ depends on the spatial coordinate $\mathbf{r} \in R \subset \mathbb{R}^d$ ($d = 3$ for most practical applications) and on the direction $\mathbf{s} \in S^{d-1}$, with S^{d-1} denoting the unit sphere in \mathbb{R}^d . The gradient appearing in (1.1) is taken with respect to \mathbf{r} only. The physical properties of the medium covered by R enter (1.1) through the total attenuation (or transport) coefficient $\sigma_t(\mathbf{r}) := \sigma_a(\mathbf{r}) + \sigma_s(\mathbf{r})$, which accounts for the absorption and scattering rates, respectively, and through the scattering kernel $\theta(\mathbf{s} \cdot \mathbf{s}')$, which describes the probability of scattering from direction \mathbf{s}' into direction \mathbf{s} . Internal sources of radiation are modeled by the function $q(\mathbf{r}, \mathbf{s})$. We complement (1.1) by non-homogeneous inflow boundary conditions

$$(1.2) \quad u(\mathbf{r}, \mathbf{s}) = q_\partial(\mathbf{r}, \mathbf{s}) \quad \text{for } (\mathbf{r}, \mathbf{s}) \in \partial D_- := \{(\mathbf{r}, \mathbf{s}) \in \partial R \times S^{d-1} : \mathbf{n}(\mathbf{r}) \cdot \mathbf{s} < 0\},$$

with incoming intensity specified by q_∂ . Here $\mathbf{n}(\mathbf{r})$ denotes the outward normal unit vector field for a point $\mathbf{r} \in \partial R$. We refer to [9] for further details on the derivation of the radiative transfer equation. If $\theta(\mathbf{s} \cdot \mathbf{s}') = 1/|S^{d-1}|$, scattering is called isotropic; otherwise, anisotropic.

1.1. Approach and contribution. A common approach for showing well-posedness of (1.1) is to prove convergence of the following iterative scheme: Given z_0 , compute the solution z_{k+1} to

$$(1.3) \quad \mathbf{s} \cdot \nabla z_{k+1} + \sigma_t z_{k+1} = \sigma_s \int_{S^{d-1}} \theta(\mathbf{s} \cdot \mathbf{s}') z_k d\mathbf{s}' + q \quad \text{in } D,$$

^{*}Department of Applied Mathematics, University of Twente, P.O. Box 217, 7500 AE Enschede, The Netherlands. r.bardin@utwente.nl.

[†]Department of Applied Mathematics, University of Twente, P.O. Box 217, 7500 AE Enschede, The Netherlands. m.schlottbom@utwente.nl

with $z_{k+1} = q_\partial$ on ∂D_- for $k \geq 0$ [1]. Under the condition that $\rho := \sup_{\mathbf{r}} \sigma_s(\mathbf{r})/\sigma_t(\mathbf{r}) < 1$ one obtains linear convergence of z_k towards u with rate ρ [8]; for more general conditions, see also [13]. Since in many applications mentioned above $\rho \approx 1$, the convergence of z_k to u is prohibitively slow. From a numerical point of view, (1.3) serves as a starting point for constructing iterative solvers for discretizations of (1.1).

In this paper we propose to accelerate the convergence of (1.3) through residual minimization over suitable subspaces. Specifically, in analogy to (1.3), given u_k , we compute in a first step the solution $u_{k+1/2}$ to

$$(1.4) \quad \mathbf{s} \cdot \nabla u_{k+1/2} + \sigma_t u_{k+1/2} = \sigma_s \int_{S^{d-1}} \theta(\mathbf{s} \cdot \mathbf{s}') u_k d\mathbf{s}' + q, \quad \text{in } D,$$

with $u_{k+1/2} = q_\partial$ on ∂D_- . To proceed, let us introduce the residual

$$(1.5) \quad \tilde{r}_k := \tilde{\mathcal{R}}(u_k) := q - \left(\mathbf{s} \cdot \nabla u_k + \sigma_t u_k - \sigma_s \int_{S^{n-1}} \theta(\mathbf{s} \cdot \mathbf{s}') u_k d\mathbf{s}' \right),$$

and the preconditioned residual $r_k := \mathcal{R}(u_k)$ that is defined as the solution to

$$(1.6) \quad \mathbf{s} \cdot \nabla r_k + \sigma_t r_k = \tilde{r}_k \quad \text{in } D, \quad r_k = 0 \text{ on } \partial D_-.$$

We note that $\mathcal{R}(u_k) = u_{k+1/2} - u_k$. Using the weighted L^2 -norm $\|v\|_{\sigma_t} := \|\sqrt{\sigma_t} v\|_{L^2(D)}$, we will show in Lemma 3.2 below the following monotonicity result for the preconditioned residual.

LEMMA 1.1. *For $k \geq 0$ let u_k , $u_{k+1/2}$ be related by (1.4) and denote $r_k = \mathcal{R}(u_k)$ and $r_{k+1/2} = \mathcal{R}(u_{k+1/2})$ the respective preconditioned residuals defined in (1.6). Then it holds that*

$$\|r_{k+1/2}\|_{\sigma_t} \leq \rho \|r_k\|_{\sigma_t}.$$

In view of the monotonicity of the residuals, we look for a correction to the intermediate iterate $u_{k+1/2}$ by residual minimization, i.e.,

$$(1.7) \quad u_{k+1/2}^c := \operatorname{argmin}_{v \in W_N} \|\mathcal{R}(u_{k+1/2} + v)\|_{\sigma_t},$$

where W_N is a suitable finite-dimensional linear space of dimension N , and set

$$(1.8) \quad u_{k+1} := u_{k+1/2} + u_{k+1/2}^c.$$

Using the minimization property and the equivalence between the residual and the error, we will show our main convergence statement.

THEOREM 1.2. *For any initial guess $u_0 \in L^2(D)$, the sequence $\{u_k\}$ defined via (1.4) and (1.8) converges linearly to the solution u of (1.1) with rate ρ , i.e.,*

$$(1.9) \quad \|u - u_k\|_{\sigma_t} \leq \frac{\rho^k}{1 - \rho} \|r_0\|_{\sigma_t}, \quad k \geq 0.$$

In general, as shown numerically below, the theoretical bound in (1.9) is too pessimistic, because it does not show the dependence on W_N . Indeed, by choosing $W_N = \{0\}$, we obtain $u_k = z_k$ if $u_0 = z_0$, and the bound in (1.9) resembles the error estimate for the iteration defined through (1.3).

However, we highlight the robust convergence of the proposed scheme for any choice of W_N . For example, W_N may contain previous iterates, which allows us to relate (1.4), (1.8) to preconditioned GMRES methods or Anderson acceleration techniques, cf. [33]. Another example is to construct W_N by solving low-dimensional diffusion problems, see Section 5 for details and Section 6 for the improved convergence behavior, where we particularly consider high-order diffusion problems for highly anisotropic scattering.

The outlined approach serves as a blueprint for constructing discrete schemes. To do so, we will employ suitable (Galerkin) discretization schemes such that the monotonicity properties of the residuals are automatically guaranteed. In view of the inversion of the transport term in (1.4), we will particularly focus on discontinuous Galerkin discretizations in \mathbf{s} considered in [11], which allow for straightforward parallelization. Such discretizations inherit similar convergence properties as the iteration described above. This general framework can be related to existing work, as discussed next.

1.2. Related works. The scheme (1.3) has been combined with several discretization methods to obtain a practical solver for radiative transfer problems. These numerical schemes are typically local in \mathbf{s} , such as the discrete ordinates method, also known as S_N -method. We refer to [1, 19] for an overview of classical approaches and well-established references, and to [23, 28, 31] for more recent strategies. The main drawback of (1.3) is the well-known slow convergence for $\rho \approx 1$. Several approaches for the acceleration of (1.3) have been proposed in the literature, cf. [1, 19] for a discussion. As observed in [1], (1.3) is a preconditioned Richardson iteration for solving (1.1). One approach to obtain faster convergence is to employ more effective preconditioners. Among the most popular ones, we mention preconditioners that are based on solving (non-)linear diffusion problems, which are well motivated by asymptotic analysis, see again, e.g., [1] for classical approaches, or [2, 34] for more recent developments.

The success of diffusion-based acceleration schemes hinges on so-called *consistent* discretization of (1.1) and the corresponding diffusion problem [1]. In [24] consistent correction equations are obtained for two-dimensional problems with anisotropic scattering by using a modified interior penalty discontinuous Galerkin approximation for the diffusion problem. The corresponding acceleration scheme is, however, less effective for highly heterogeneous optical parameters. A discrete analysis of similar methods for high-order discontinuous Galerkin discretizations can be found in [15]. We refer also to [29] for the development of preconditioners for heterogeneous media. Instead of constructing special discretizations for the diffusion problems for each discretization scheme of (1.1), consistent discretizations can automatically be obtained by using subspace corrections of suitable Galerkin approximations of (1.1) [11, 21, 22]. In [21] isotropic scattering problems have been solved for a discrete ordinates-discontinuous Galerkin discretization using nonlinear diffusion problems and Anderson acceleration. The approach presented in [21] reduces the full transport problem to a nonlinear diffusion equation for the angular average only, which is, however, not possible for anisotropic scattering. The approach taken in [11] for anisotropic scattering problems employs a positive definite, self-adjoint second-order form of (1.1), which facilitates the convergence analysis, but it requires another iterative method to actually apply the resulting matrices. The approach taken here avoids such extra inner iterations at the expense of dealing with indefinite problems. The flexibility of our approach in constructing the spaces W_N for the residual minimization allows us to employ similar subspaces as in [11], which have been shown to converge robustly for arbitrary meshes and for forward-peaked scattering.

To treat forward-peaked scattering, for a one-dimensional radiative transfer equation, [36] applies nonlinear diffusion correction and Anderson acceleration, which minimizes the residual over

a certain subspace, and is therefore conceptually close to our approach outlined above. Different from [36], where a combination of the S_N -method with a finite difference method for the discretization of \mathbf{r} has been used and the corresponding minimizations are done in the Euclidean norm, our framework allows for general discretizations for multi-dimensional problems, such as arbitrary order (discontinuous) Galerkin schemes, to discretize \mathbf{s} and \mathbf{r} . Moreover, our framework allows us to employ higher-order correction equations, similar to [11], whose effectiveness becomes apparent in our numerical examples for highly forward-peaked scattering. In addition, our Hilbert space approach, which is provably convergent, leads to algorithms that behave robustly under mesh refinements.

A second approach for accelerating (1.3) is to replace the preconditioned Richardson iterations with other Krylov space methods. For instance, [35] employs a GMRES method, which is preconditioned by solving a diffusion problem, to solve three-dimensional problems with isotropic scattering. To treat highly forward-peaked scattering, [32] combines GMRES with an angular (in the \mathbf{s} variable) multigrid method to accelerate convergence; see also [17, 18], and [10] for a comparison of multilevel approaches. By appropriately choosing W_N in (1.7) the approach outlined in Subsection 1.1 can be related to a preconditioned GMRES method. Since the domain D has dimension $2d - 1$, building up a full Krylov space during GMRES iterations becomes prohibitive in terms of memory, and GMRES has to be restarted. Our numerical results, cf. also [11], show that high-order diffusion corrections can lead to effective schemes with small memory requirements for highly forward-peaked scattering.

1.3. Outline. The remainder of the manuscript is organized as follows. In Section 2 we introduce notation and basic assumptions on the optical parameters, and we present a weak formulation of (1.1), (1.2), which allows for a rigorous proof of Lemma 1.1 in Section 3. In Section 4 we turn to the analysis of the minimization problem (1.7) and prove Theorem 1.2. In Section 5 we discuss a discretization strategy that implements the approach described in Subsection 1.1 such that our main convergence results remain true for the discrete systems. We discuss several choices of W_N there. The practical performance of the proposed methodology for different choices of spaces W_N in (1.7) is investigated in Section 6.

2. Notation and preliminaries. In the following, we recall the main functional analytic framework and state the variational formulation of (1.1)-(1.2), with a well-posedness result.

2.1. Function spaces. We denote with $V_0 := L^2(D)$ the usual Hilbert space of square integrable functions on the domain $D := R \times S^{d-1}$, with inner product (\cdot, \cdot) and induced norm $\|\cdot\|$. In order to incorporate boundary conditions, we assume that R has a Lipschitz boundary and we denote with $L^2(\partial D_-; |\mathbf{s} \cdot \mathbf{n}|)$ the space of weighted square-integrable functions on the inflow boundary, and with $(\cdot, \cdot)_{\partial D_-}$ the corresponding inner product. For smooth functions $v, w \in C^\infty(\bar{D})$ we define

$$(2.1) \quad (v, w)_{V_1} := (v, w) + (\mathbf{s} \cdot \nabla v, \mathbf{s} \cdot \nabla w) + (|\mathbf{s} \cdot \mathbf{n}|v, w)_{\partial D_-},$$

and we denote with V_1 the completion of $C^\infty(\bar{D})$ with respect to the norm associated with (2.1):

$$V_1 = \{v \in V_0 : \mathbf{s} \cdot \nabla v \in V_0, v|_{\partial D_-} \in L^2(\partial D_-; |\mathbf{s} \cdot \mathbf{n}|)\}.$$

For functions $v, w \in V_1$, we recall the following integration by parts formula, see, e.g., [12],

$$(2.2) \quad (\mathbf{s} \cdot \nabla v, w) = -(v, \mathbf{s} \cdot \nabla w) + (\mathbf{s} \cdot \mathbf{n}v, w)_{\partial D_-}.$$

2.2. Optical parameters and data. Standard assumptions for the source data are $q \in V_0$ and $q_\partial \in L^2(\partial D_-; |\mathbf{s} \cdot \mathbf{n}|)$. The optical parameters σ_s and σ_t are supposed to be positive and essentially bounded functions of \mathbf{r} . The medium R is assumed to be absorbing, i.e., there exists $c_0 > 0$ such that $\sigma_a \geq c_0$ a.e. in R . This hypothesis ensures that the ratio between the scattering rate and the total attenuation rate is strictly less than 1, i.e., $\rho := \|\sigma_s/\sigma_t\|_\infty < 1$. We assume that the phase function $\theta : [-1, 1] \rightarrow \mathbb{R}$ is non-negative and normalized such that $\int_{S^{d-1}} \theta(\mathbf{s} \cdot \mathbf{s}') d\mathbf{s}' = 1$ for a.e. $\mathbf{s} \in S^{d-1}$. To ease the notation we introduce the operators $\mathcal{S}, \Theta : V_0 \rightarrow V_0$ such that

$$(\mathcal{S}v)(\mathbf{r}, \mathbf{s}) := \sigma_s(\mathbf{r})(\Theta v)(\mathbf{r}, \mathbf{s}), \quad (\Theta v)(\mathbf{r}, \mathbf{s}) := \int_{S^{d-1}} \theta(\mathbf{s} \cdot \mathbf{s}') v(\mathbf{r}, \mathbf{s}') d\mathbf{s}'.$$

We recall that \mathcal{S}, Θ are self-adjoint bounded linear operators, with operator norms bounded by $\|\sigma_s\|_\infty$ and 1, respectively, i.e., $\|\Theta v\|_{V_0} \leq \|v\|_{V_0}$, see, e.g., [12, Lemma 2.6].

2.3. Even-odd splitting. For $v \in V_0$, we define its even and odd parts, identified by the superscripts " + " and " - ", respectively, by

$$v^\pm(\mathbf{r}, \mathbf{s}) := \frac{1}{2} (v(\mathbf{r}, \mathbf{s}) \pm v(\mathbf{r}, -\mathbf{s})).$$

Accordingly, for any space V we denote by $V^\pm := \{v^\pm : v \in V\}$ the subspaces of even and odd functions of V . In particular, any $V \in \{V_0, V_1\}$ has the orthogonal (with respect to the inner product of V) decomposition $V = V^+ \oplus V^-$. Following [12], a suitable space for the analysis of the radiative transfer equation is the space of mixed regularity

$$W := V_1^+ \oplus V_0^-,$$

where only the even components have weak directional derivatives in V_0 .

2.4. Variational formulation. Assuming that u is a smooth solution to (1.1)-(1.2), we use standard procedures to derive a weak formulation. Multiplying (1.1) by a smooth test function v , splitting the functions in their even and odd components, and using the integration by parts formula (2.2) to handle the term $(\mathbf{s} \cdot \nabla u^-, v^+)$, we obtain the following variational principle, see [12] for details: find $u \in W$ such that for all $v \in W$

$$(2.3) \quad t(u, v) = s(u, v) + \ell(v),$$

with bilinear forms $t, s : W \times W \rightarrow \mathbb{R}$, and linear form $\ell : W \rightarrow \mathbb{R}$ defined by

$$(2.4) \quad t(u, v) := (\mathbf{s} \cdot \nabla u^+, v^-) - (u^-, \mathbf{s} \cdot \nabla v^+) + (\sigma_t u, v) + (|\mathbf{s} \cdot \mathbf{n}| u^+, v^+)_{\partial D},$$

$$(2.5) \quad s(u, v) := (\mathcal{S}u, v),$$

$$(2.6) \quad \ell(v) := (q, v) - 2(\mathbf{s} \cdot \mathbf{n} q_\partial, v^+)_{\partial D_-}.$$

As shown in [12, Section 3] the assumptions imposed in Subsection 2.2 imply that there exists a unique solution of (2.3) satisfying

$$\|u\|_W \leq C(\|q\| + \|q_\partial\|_{L^2(\partial D_-; |\mathbf{s} \cdot \mathbf{n}|)}),$$

with constant $C > 0$ depending only on c_0 and $\|\sigma_t\|_\infty$. Let us also recall from [12] that the odd part of the weak solution $u \in W$ enjoys $u^- \in V_1$, and that u satisfies (1.1) almost everywhere, and

(1.2) in the sense of traces. Before proceeding, we collect some properties of the bilinear forms s and t , which we will use in our analysis below.

LEMMA 2.1. *Let $\rho = \|\sigma_s/\sigma_t\|_\infty$. For any $u, v \in W$ the following inequalities hold:*

$$(2.7) \quad \|u\|_{\sigma_t}^2 \leq t(u, u),$$

$$(2.8) \quad s(u, v) \leq \rho \|u\|_{\sigma_t} \|v\|_{\sigma_t}.$$

Proof. The inequality (2.7) follows immediately from (2.4) and the definition of the weighted norm. To show (2.8) we apply the Cauchy-Schwarz inequality to obtain that

$$s(u, v) = \left(\frac{\sigma_s}{\sigma_t} \Theta(\sqrt{\sigma_t} u), \sqrt{\sigma_t} v \right) \leq \rho \|\Theta(\sqrt{\sigma_t} u)\| \|\sqrt{\sigma_t} v\| \leq \rho \|u\|_{\sigma_t} \|v\|_{\sigma_t},$$

where we used the boundedness of Θ in the last step. \square

3. Contraction properties of the source iteration. Equipped with the notation from the previous section, we can write (1.4) as follows: Given $u_k \in W$, compute $u_{k+1/2} \in W$ such that

$$(3.1) \quad t(u_{k+1/2}, v) = s(u_k, v) + \ell(v), \quad \forall v \in W.$$

The following result is well-known, and we provide a proof for later reference.

LEMMA 3.1. *Let $u_k, u_{k+1/2} \in W$ be related via (3.1). Then it holds that*

$$\|u - u_{k+1/2}\|_{\sigma_t} \leq \rho \|u - u_k\|_{\sigma_t},$$

with $\rho = \|\sigma_s/\sigma_t\|_\infty$.

Proof. Abbreviating $e_{k+1/2} := u - u_{k+1/2}$ and $e_k := u - u_k$, (2.3) and (3.1) imply that

$$(3.2) \quad t(e_{k+1/2}, v) = s(e_k, v), \quad \forall v \in W.$$

Therefore, setting $v = e_{k+1/2}$ in (3.2), using (2.7) and (2.8), we obtain the estimates

$$\|e_{k+1/2}\|_{\sigma_t}^2 \leq t(e_{k+1/2}, e_{k+1/2}) = s(e_k, e_{k+1/2}) \leq \rho \|e_{k+1/2}\|_{\sigma_t} \|e_k\|_{\sigma_t},$$

which concludes the proof. \square

Along the lines of (1.5) and (1.6), we define the residual operator $\tilde{\mathcal{R}} : W \rightarrow W^*$ by

$$\langle \tilde{\mathcal{R}}(w), v \rangle := \ell(v) - (t(w, v) - s(w, v)), \quad \forall v \in W.$$

Here, W^* denotes the dual space of W , and $\langle \cdot, \cdot \rangle$ the corresponding duality pairing. The dual norm is defined by $\|\ell\|_{W^*} := \sup_{\|v\|_W=1} \ell(v)$. The preconditioned residual operator $\mathcal{R} : W \rightarrow W$ is defined by solving the following transport problem without scattering,

$$t(\mathcal{R}(w), v) = \langle \tilde{\mathcal{R}}(w), v \rangle, \quad \forall v \in W.$$

Using the arguments used to analyze (2.3) in Subsection 2.4, one shows that the operator \mathcal{R} is well-defined. The following result ensures that the corresponding preconditioned residuals decay monotonically, which verifies Lemma 1.1.

LEMMA 3.2. Let $u_k, u_{k+1/2} \in W$ be related via (3.1). Then it holds that

$$\|\mathcal{R}(u_{k+1/2})\|_{\sigma_t} \leq \rho \|\mathcal{R}(u_k)\|_{\sigma_t}.$$

Proof. Denoting $r_k = \mathcal{R}(u_k)$ and using (3.2), we observe that

$$\begin{aligned} t(r_k, v) &= \langle \tilde{\mathcal{R}}(u_k), v \rangle = \ell(v) - (t(u_k, v) - s(u_k, v)) \\ &= t(e_k, v) - s(e_k, v) = t(e_k, v) - t(e_{k+1/2}, v) \\ &= t(u_{k+1/2} - u_k, v), \end{aligned}$$

for all $v \in W$, i.e., $r_k = u_{k+1/2} - u_k$. Using a similar argument and (3.2), we further obtain that

$$\begin{aligned} t(r_{k+1/2}, v) &= \langle \tilde{\mathcal{R}}(u_{k+1/2}), v \rangle = \ell(v) - (t(u_{k+1/2}, v) - s(u_{k+1/2}, v)) \\ &= t(e_{k+1/2}, v) - s(e_{k+1/2}, v) = s(e_k, v) - s(e_{k+1/2}, v) \\ &= s(u_{k+1/2} - u_k, v) = s(r_k, v), \end{aligned}$$

for all $v \in W$. In view of the proof of Lemma 3.1, the proof is complete. \square

The following result allows us to relate the error to the residual quantitatively.

LEMMA 3.3. Let $u \in W$ be the solution to (2.3). Then the following estimate holds

$$\|u - w\|_{\sigma_t} \leq \frac{1}{1 - \rho} \|\mathcal{R}(w)\|_{\sigma_t} \quad \forall w \in W.$$

Proof. Let us introduce the linear operator $\mathcal{R}_0 : W \rightarrow W$ defined by $\mathcal{R}_0 w := \mathcal{R}(w) - L$, where $L \in W$ is defined by the relation $t(L, v) = \ell(v)$, for $v \in W$. We observe that for $v \in W$, inequality (2.7), the definition of \mathcal{R} and (2.8) imply that

$$\|\mathcal{R}_0 v + v\|_{\sigma_t}^2 \leq t(\mathcal{R}_0 v + v, \mathcal{R}_0 v + v) = s(v, \mathcal{R}_0 v + v) \leq \rho \|v\|_{\sigma_t} \|\mathcal{R}_0 v + v\|_{\sigma_t}.$$

The triangle inequality thus implies that $\|v\|_{\sigma_t} \leq \|v + \mathcal{R}_0 v\|_{\sigma_t} + \|\mathcal{R}_0 v\|_{\sigma_t} \leq \rho \|v\|_{\sigma_t} + \|\mathcal{R}_0 v\|_{\sigma_t}$, i.e.,

$$(3.3) \quad \|v\|_{\sigma_t} \leq \|\mathcal{R}_0 v\|_{\sigma_t} / (1 - \rho) \quad \forall v \in W.$$

The assertion follows from (3.3) with $v = u - w$ and the observation that $\mathcal{R}_0(u - w) = -\mathcal{R}(w)$. \square

4. Residual minimization. In view of Lemma 3.3 the difference between the weak solution u of (2.3) and any element $w \in W$ is bounded from above by the norm of the residual $\mathcal{R}(w)$ associated with w . Hence, if we can construct w such that $\mathcal{R}(w) = 0$, then $u = w$. Lemma 3.2 shows that the half-step (3.2) reduces the norm of the residual by the factor ρ . These observations motivate us to modify $u_{k+1/2}$ such that the corresponding residual becomes smaller. In order to obtain a feasible minimization problem, let $W_N \subset W$ be a subspace of finite dimension N . We then compute the modification $u_{k+1/2}^c \in W_N$ such that

$$(4.1) \quad u_{k+1/2}^c := \operatorname{argmin}_{w \in W_N} \|\mathcal{R}(u_{k+1/2} + w)\|_{\sigma_t}^2.$$

The new iterate of the scheme is then defined as

$$(4.2) \quad u_{k+1} := u_{k+1/2} + u_{k+1/2}^c,$$

and the procedure can restart.

LEMMA 4.1. *The minimization problem in (4.1) has a unique solution $u_{k+1/2}^c \in W_N$.*

Proof. Since $\mathcal{R}(u_{k+1/2} + w) = \mathcal{R}(u_{k+1/2}) + \mathcal{R}_0 w$ with \mathcal{R}_0 as defined in the proof of Lemma 3.3, the optimization problem (4.1) is a least-squares problem for the norm $\|\cdot\|_{\sigma_t}^2$ with linear operator \mathcal{R}_0 and data $-\mathcal{R}(u_{k+1/2})$. A necessary condition for a minimizer $w^* \in W_N$ is therefore

$$(4.3) \quad (\mathcal{R}_0 w^*, \mathcal{R}_0 v)_{\sigma_t} = -(\mathcal{R}(u_{k+1/2}), \mathcal{R}_0 v)_{\sigma_t} \quad \forall v \in W_N.$$

In view of (3.3), the minimizer $u_{k+1/2}^c = w^*$ is unique, and hence exists, because W_N is finite dimensional and (4.3) is a quadratic problem. \square

Proof of Theorem 1.2. Using Lemma 3.3, the minimization property of u_{k+1} , and Lemma 3.2 we obtain that

$$(1 - \rho)\|e_{k+1}\|_{\sigma_t} \leq \|\mathcal{R}(u_{k+1})\|_{\sigma_t} \leq \rho^{k+1}\|\mathcal{R}(u_0)\|_{\sigma_t},$$

which concludes the proof.

5. Numerical realization. The convergent iteration in infinite-dimensional Hilbert spaces described in the previous sections serves as a blueprint for constructing numerical methods. The variational character of the scheme allows translating the infinite-dimensional iteration directly to a corresponding convergent iteration in finite-dimensional approximation spaces W_h of W .

5.1. Galerkin approximation. To be specific, we employ for W_h a construction as in [11]. Let \mathcal{T}_h^R and \mathcal{T}_h^S be shape regular, quasi-uniform and conforming triangulations of R and S , respectively. Here, $h > 0$ denotes a mesh-size parameter. In addition, we require that $-K^S \in \mathcal{T}_h^S$ for any $K^S \in \mathcal{T}_h^S$ in order to be able to properly handle even and odd functions. We then denote by S_h^\pm the corresponding finite element spaces of even piecewise constant (+) and odd piecewise linear (−) functions associated with \mathcal{T}_h^S . Similarly, we denote by X_h^\pm the finite element spaces consisting of piecewise constant (−) and continuous piecewise linear (+) functions associated with \mathcal{T}_h^R . Please note that we use the symbol \pm in X_h^\pm for notational convenience and not to indicate whether a function of the spatial variable is even or odd. Our considered approximation space is then defined as $W_h = S_h^+ \otimes X_h^+ + S_h^- \otimes X_h^-$. The Galerkin approximation of (2.3) reads: Find $u_h \in W_h$ such that

$$(5.1) \quad t(u_h, v_h) = s(u_h, v_h) + \ell(v_h) \quad \forall v_h \in W_h.$$

As shown in [12], (5.1) has a unique solution $u_h \in W_h$ that is uniformly (in h) bounded by $\|\ell\|_{W^*}$. Moreover, there is a constant $C > 0$ independent of the discretization parameters such that

$$\|u - u_h\|_W \leq C \inf_{v_h \in W_h} \|u - v_h\|_W,$$

i.e., u_h is a quasi-best approximation to u in W_h .

5.2. Iterative scheme. The discretization of (3.1), (4.2) becomes: Given $u_{h,k} \in W_h$, compute $u_{h,k+1/2} \in W_h$ such that

$$(5.2) \quad t(u_{h,k+1/2}, v_h) = s(u_{h,k}, v_h) + \ell(v_h), \quad \forall v_h \in W_h.$$

The discretization of the preconditioned residual operator is $\mathcal{R}_h : W_h \rightarrow W_h$ defined via

$$t(\mathcal{R}_h(w_h), v_h) = \ell(v_h) - (t(w_h, v_h) - s(w_h, v_h)), \quad \forall v_h \in W_h,$$

and the corresponding corrections are computed via the minimization problem

$$(5.3) \quad u_{h,k+1/2}^c := \operatorname{argmin}_{w_h \in W_{h,N}} \|\mathcal{R}_h(u_{h,k+1/2} + w_h)\|_{\sigma_t}^2,$$

where $W_{h,N} \subset W_h$. The new iterate of the discrete scheme is then defined accordingly by

$$(5.4) \quad u_{h,k+1} := u_{h,k+1/2} + u_{h,k+1/2}^c.$$

Repeating the arguments of [Section 3](#) and [Section 4](#), we obtain the following convergence statement.

THEOREM 5.1. *For any $u_{h,0} \in W_h$, the sequence $\{u_{h,k}\}$ defined by (5.2), (5.4) converges linearly to the solution u_h of (5.1), i.e.,*

$$\|u_h - u_{h,k}\|_{\sigma_t} \leq \frac{\rho^k}{1 - \rho} \|\mathcal{R}_h(u_{h,0})\|_{\sigma_t}.$$

Moreover, the residuals converge monotonically, i.e., $\|\mathcal{R}_h(u_{h,k+1})\|_{\sigma_t} \leq \rho \|\mathcal{R}_h(u_{h,k})\|_{\sigma_t}$.

5.3. Formulation in terms of matrices. Choosing basis functions for S_h^\pm and X_h^\pm allows us to rewrite the iteration $u_{h,k} \mapsto u_{h,k+1}$ in corresponding coordinates. Denote $\{\varphi_i\}_{i=1}^{n_R^+}$ and $\{\chi_j\}_{j=1}^{n_R^-}$ the usual basis functions with local support of X_h^+ and X_h^- , i.e., φ_i vanishes in all vertices of \mathcal{T}_h^R except in the i th one, while χ_j vanishes in all elements of \mathcal{T}_h^R except in the j th one. Similarly, we denote $\{\mu_k\}$ the basis of S_h^+ such that μ_k vanishes in all elements of \mathcal{T}_h^S except in K_k^S and $-K_k^S$. Eventually, we denote by $\{\psi_l\}_{l=1}^{n_S^-}$ the basis of S_h^- such that ψ_l vanishes in all vertices belonging to \mathcal{T}_h^S except for the vertices p_l and $-p_l$. We may then write the even and odd parts of u_h as

$$u_h^+ = \sum_{i=1}^{n_R^+} \sum_{k=1}^{n_S^+} \mathbf{u}_{i,k}^+ \varphi_i \mu_k, \quad u_h^- = \sum_{j=1}^{n_R^-} \sum_{l=1}^{n_S^-} \mathbf{u}_{j,l}^- \chi_j \psi_l,$$

and (5.1) turns into the linear system

$$(5.5) \quad \mathbf{T}\mathbf{u} = \mathbf{S}\mathbf{u} + \mathbf{l}$$

with matrices \mathbf{T} and \mathbf{S} having the following block structure,

$$(5.6) \quad \mathbf{T} := \begin{bmatrix} \mathbf{B} + \mathbf{M}^+ & -\mathbf{A}^T \\ \mathbf{A} & \mathbf{M}^- \end{bmatrix}, \quad \mathbf{S} := \begin{bmatrix} \mathbf{S}^+ & \\ & \mathbf{S}^- \end{bmatrix}, \quad \mathbf{l} := \begin{bmatrix} \mathbf{l}^+ \\ \mathbf{l}^- \end{bmatrix}.$$

The individual blocks are given as follows:

$$\begin{aligned} \mathbf{S}^+ &:= \boldsymbol{\Theta}^+ \otimes \mathbf{M}_{\sigma_s}^+, & \mathbf{S}^- &:= \boldsymbol{\Theta}^- \otimes \mathbf{M}_{\sigma_s}^-, \\ \mathbf{M}^+ &:= \mathbf{M}^+ \otimes \mathbf{M}_{\sigma_t}^+, & \mathbf{M}^- &:= \mathbf{M}^- \otimes \mathbf{M}_{\sigma_t}^-, \\ \mathbf{A} &:= \sum_{i=1}^d \mathbf{A}_i \otimes \mathbf{D}_i, & \mathbf{B} &:= \operatorname{blkdiag}(\mathbf{B}_1, \dots, \mathbf{B}_{n_S^+}), \end{aligned}$$

with matrices

$$\begin{aligned}
(\mathbf{M}_{\sigma_s}^+)_{i,i'} &:= \int_R \sigma_i \varphi_i \varphi_{i'} d\mathbf{r}, & (\boldsymbol{\Theta}^+)_{k,k'} &:= \int_S \int_S \theta(\mathbf{s} \cdot \mathbf{s}') \mu_k(\mathbf{s}') \mu_{k'}(\mathbf{s}) d\mathbf{s}' d\mathbf{s}, \\
(\mathbf{M}_{\sigma_s}^-)_{j,j'} &:= \int_R \sigma_j \chi_j \chi_{j'} d\mathbf{r}, & (\boldsymbol{\Theta}^-)_{l,l'} &:= \int_S \int_S \theta(\mathbf{s} \cdot \mathbf{s}') \psi_l(\mathbf{s}') \psi_{l'}(\mathbf{s}) d\mathbf{s}' d\mathbf{s}, \\
(\mathbf{D}_n)_{i,k} &:= \int_R \frac{\partial \varphi_i}{\partial r_n} \chi_k d\mathbf{r}, & (\mathbf{A}_i)_{l,k} &:= \int_S \mathbf{s}_i \psi_l \mu_k d\mathbf{s}, \\
(\mathbf{B}_k)_{i,i'} &:= \int_{\partial R} \varphi_i \varphi_{i'} \omega_k d\mathbf{r}, & \omega_k &:= \int_S |\mathbf{s} \cdot \mathbf{n}| (\mu_k)^2 d\mathbf{s}, \\
(\mathbf{M}^+)_{k,k'} &:= \int_S \mu_k \mu_{k'} d\mathbf{s}, & (\mathbf{M}^-)_{l,l'} &:= \int_S \psi_l \psi_{l'} d\mathbf{s}.
\end{aligned}$$

The vectors \mathbf{l}^\pm are obtained from inserting basis functions into the linear functional ℓ . We mention that all matrices are sparse, except $\boldsymbol{\Theta}^+$ and $\boldsymbol{\Theta}^-$, which can be applied efficiently using hierarchical matrix compression, see [11] – for moderate n_S^+ , n_S^- dense linear algebra is efficient, too. In particular, the matrices $\mathbf{M}_{\sigma_s}^-$ and \mathbf{M}^- are diagonal and 3×3 block diagonal, respectively, i.e., \mathbf{M}^- can be inverted efficiently. Using these matrices, (5.2) turns into the linear system

$$(5.7) \quad \mathbf{T} \mathbf{u}_{k+1/2} = \mathbf{S} \mathbf{u}_k + \mathbf{l},$$

which can be solved as described in Remark 5.2. Denote $\mathbf{R}(\mathbf{w})$ the coordinate vector of $\mathcal{R}_h(w)$. Then $\mathbf{R}(\mathbf{w})$ is determined by solving

$$\mathbf{T} \mathbf{R}(\mathbf{w}) = \mathbf{l} - (\mathbf{T} - \mathbf{S}) \mathbf{w}.$$

Hence, the operator \mathcal{R}_{h_0} discretizing \mathcal{R}_0 becomes $\mathbf{R}_0 \mathbf{w} = \mathbf{R}(\mathbf{w}) - \mathbf{R}(0)$. The update is computed via the minimization (5.3), which becomes, cf. (4.3),

$$(5.8) \quad (\mathbf{R}_0^N)^T \mathbf{M} \mathbf{R}_0^N \mathbf{w}^* = -(\mathbf{R}_0^N)^T \mathbf{M} \mathbf{R}(\mathbf{u}_{k+1/2}),$$

where $\mathbf{M} = \text{blkdiag}(\mathbf{M}^+, \mathbf{M}^-)$. Here, $\mathbf{R}_0^N = \mathbf{R}_0 \mathbf{W}_{h,N}$, where $\mathbf{W}_{h,N}$ is a matrix, whose columns correspond to the coordinates of a basis for $W_{h,N}$. Depending on the conditioning of the matrix $\mathbf{W}_{h,N}$, the system in (5.8) might be ill-conditioned. To stabilize the solution process, we compute the minimum-norm solution. The coordinate vector for the correction $u_{h,k+1/2}^c$ is then given by $\mathbf{u}_{k+1/2}^c = \mathbf{W}_{h,N} \mathbf{w}^*$, which gives the following update formula for the coordinates of the new iterate

$$(5.9) \quad \mathbf{u}_{k+1} = \mathbf{u}_{k+1/2} + \mathbf{u}_{k+1/2}^c.$$

The residual corresponding to $u_{h,k+1}$ can be updated according to $\mathbf{r}_{k+1} = \mathbf{R} \mathbf{u}_{k+1/2} + \mathbf{R}_0^N \mathbf{w}^*$. Theorem 5.1 ensures that \mathbf{u}_k converges linearly to the solution \mathbf{u} of (5.5).

Remark 5.2. Solving for $\mathbf{u}_{k+1/2}$ can be done in two steps. First, one may solve the symmetric positive definite system

$$(5.10) \quad (\mathbf{A}^T (\mathbf{M}^-)^{-1} \mathbf{A} + \mathbf{M}^+ + \mathbf{B}) \mathbf{u}_{k+1/2}^+ = \mathbf{S}^+ \mathbf{u}_k^+ + \mathbf{l}^+ + \mathbf{A}^T (\mathbf{M}^-)^{-1} (\mathbf{l}^- + \mathbf{S}^- \mathbf{u}_k^-).$$

The system in (5.10) is block diagonal with n_S^+ many sparse blocks of size $n_R^+ \times n_R^+$ and can be solved in parallel, with straightforward parallelization over each element of \mathcal{T}_h^S . Second, one may then retrieve the odd part by solving the system

$$\mathbf{M}^- \mathbf{u}_{k+1/2}^- = \mathbf{S}^- \mathbf{u}_k^+ - \mathbf{A} \mathbf{u}_{k+1/2}^+ + \mathbf{l}^-,$$

which can be accomplished with linear complexity due to the structure of \mathbf{M}^- .

Remark 5.3. Assuming that the dimension of $W_{h,N}$ is N , (5.8) is a dense $N \times N$ system in general, which can be solved at negligible cost for small N . The assembly of the corresponding linear system, i.e., of the matrix \mathbf{R}_0^N and the right-hand side $\mathbf{R}(\mathbf{u}_{k+1/2}) = \mathbf{R}_0(\mathbf{u}_{k+1/2}) + \mathbf{R}(0)$, requires $N + 1$ applications of \mathbf{R}_0 , which can be carried out as described in Remark 5.2. Since we can compute $\mathbf{u}_{k+3/2} = \mathbf{u}_{k+1} + \mathbf{r}_{k+1}$ we can skip the solution of a linear system in (5.7) for $k > 0$. Hence, the computational cost for performing one step of the proposed method (5.7), (5.9) is comparable to $N + 1$ steps of a corresponding discretization of the unmodified iteration (1.3), plus the computational cost for setting up $W_{h,N}$. Thus, assuming that the cost for setting up $W_{h,N}$ is minor, the extra cost for the minimization by solving (5.8) is justified as long as the iteration (5.7), (5.9) converges faster than ρ^{N+1} .

5.4. Choice of subspaces. The previous consideration did not depend on a particular choice of the minimization space $W_{h,N}$. As discussed in Subsection 1.2, a common choice for the considered radiative transfer problem is to use corrections derived from asymptotic analysis, i.e., related diffusion problems. As has been observed in [11, 22], the corresponding discretizations of such diffusion problems can be understood as projections on constant functions in \mathbf{s} . Such functions, in turn, can be interpreted as eigenvectors of the matrix Θ^+ . Indeed, the spherical harmonics are the eigenfunctions of the integral operator in (1.1) and the lowest-order spherical harmonic is constant.

5.4.1. Constructing $W_{h,N}$ using eigenfunctions of Θ^+ . Let $\mathbf{H}_k \neq 0$ solve the generalized eigenvalue problem

$$\Theta^+ \mathbf{H}_k^+ = \gamma_k \mathbf{M}^+ \mathbf{H}_k^+,$$

for some $\gamma_k \geq 0$, where we suppose that the eigenvalues are ordered non-increasingly, i.e., $\gamma_k \geq \gamma_{k+1}$. We denote $H_{h,k}^+ \in S_h^+$ the corresponding (even) eigenfunctions, and define the space

$$H_K^+ := \text{span}\{H_{h,k}^+ : 1 \leq k \leq K\}.$$

We further define $H_{h,k,i}^- \in S_h^-$ by the relation

$$(H_{h,k,i}^-, \psi_l) = (\mathbf{s}_i H_{h,k}^+, \psi_l) \quad \text{for all } l = 1, \dots, n_S^-, \quad 1 \leq i \leq d,$$

and $H_K^- = \text{span}\{H_{h,k,i}^- : 1 \leq k \leq K, 1 \leq i \leq d\}$. Using these definitions, we can define the space

$$(5.11) \quad Y_{h,K} := H_K^+ \otimes X_h^+ + H_K^- \otimes X_h^- \subset W_h.$$

To derive a correction equation, we rewrite (3.2) as follows

$$(5.12) \quad t(u_h - u_{h,k+1/2}, v_h) = s(u_h - u_{h,k+1/2}, v_h) + s(u_{h,k+1/2} - u_{h,k}, v_h) \quad \forall v_h \in W_h.$$

Similar to [11, 22], but see also [1], we may expect to obtain a good approximation to the error $u_h - u_{h,k+1/2}$ by solving (5.12) on the subspace $Y_{h,K}$, for a certain K . We hence define $u_{h,k+1/2}^c \in Y_{h,K}$ as the unique solution of

$$(5.13) \quad t(u_{h,k+1/2}^c, v_h) = s(u_{h,k+1/2}^c, v_h) + s(u_{h,k+1/2} - u_{h,k}, v_h) \quad \forall v_h \in Y_{h,K}.$$

By construction, the space $Y_{h,K}$ satisfies the compatibility condition $\mathbf{s} \cdot \nabla y_h^+ \in Y_{h,K}^- = H_K^- \otimes X_h^-$ for any $y_h^+ \in Y_{h,K}^+$. Therefore, (5.13) has a unique solution [12]. If K is moderately small, (5.13) can be solved efficiently, see [11] for a discussion. We then define

$$(5.14) \quad W_{h,N}^c := \text{span}\{u_{h,k+1/2}^c\} \subset W_h.$$

The dimension of $W_{h,N}^c$ is $N = 1$, and (5.3) can be carried out efficiently.

Remark 5.4. Since (5.12) is a saddle-point problem, the Galerkin projection (5.13) may enlarge the error. This is in contrast to [11], where (5.1) was reformulated to a second-order form, which is symmetric and positive definite. In the latter situation, Galerkin projections correspond to best-approximations in the energy norm, and therefore do not enlarge the error.

5.4.2. Enriched space. By construction, the correction $u_{h,k+1/2}^c$ computed via solving the projected problem (5.13) does, in general, not satisfy (5.12). We will also consider enriched versions of $W_{h,N}^c$ as follows. First, we may use the corrected even iterate to find $\tilde{u}_{h,k+1/2}^{c,-} \in W_h^-$ by solving

$$\mathbf{M}^-(\mathbf{u}_{k+1/2}^- + \tilde{\mathbf{u}}_{k+1/2}^{c,-}) = \mathbf{S}^-\mathbf{u}_{k+1/2}^- + \mathbf{l}^- - \mathbf{A}(\mathbf{u}_{k+1/2}^+ + \mathbf{u}_{k+1/2}^{c,+}).$$

The (block-)diagonal structure of \mathbf{M}^- and $\mathbf{M}_{\sigma_t}^-$ allows us to invert $\mathbf{M}^- = \mathbf{M}^- \otimes \mathbf{M}_{\sigma_t}^-$ efficiently. Second, we may compute another correction as follows. Suppose that $u_{h,k+1/2}^+ + u_{h,k+1/2}^{c,+}$ is close to the even-part u_h^+ of the solution to (5.1), then, for consistency reasons, we may expect that the solution $u_{h,k+1/2}^- + \tilde{u}_{h,k+1/2}^{c,-}$ to the following system is a good approximation to u_h^- :

$$\mathbf{M}^-(\mathbf{u}_{k+1/2}^- + \tilde{\mathbf{u}}_{k+1/2}^{c,-}) = \mathbf{S}^-(\mathbf{u}_{k+1/2}^- + \tilde{\mathbf{u}}_{k+1/2}^{c,-}) + \mathbf{l}^- - \mathbf{A}(\mathbf{u}_{k+1/2}^+ + \mathbf{u}_{k+1/2}^{c,+}).$$

Computing $\tilde{\mathbf{u}}_{k+1/2}^{c,-}$ requires the inversion of $\mathbf{M}^- - \mathbf{S}^-$, which can be accomplished using a preconditioned conjugate gradient method as done in [11]. We then define the enriched space

$$(5.15) \quad \tilde{W}_{h,N}^c := \text{span}\{u_{h,k+1/2}^{c,+}, u_{h,k+1/2}^{c,-}, \tilde{u}_{h,k+1/2}^{c,-}, \tilde{\tilde{u}}_{h,k+1/2}^{c,-}\} \subset W_h,$$

which can be employed in the minimization (5.3). The dimension of this space is $N = 4$.

5.4.3. Another enriched space: including previous iterates. Since the minimization procedure is flexible in defining the correction space $W_{h,N}$, we may not only rely on minimizing the residual over functions obtained from Galerkin subspace projection. Borrowing ideas from GMRES, given an iterate $u_{h,k}$, we will also consider the space

$$(5.16) \quad \tilde{W}_{h,N}^{c,m} := \tilde{W}_{h,N}^c + \text{span}\{u_{h,j} : k - m \leq j \leq k\},$$

where also the previous m iterates are taken into account to construct the space for minimization. It is clear that if $m \geq k$ all previous iterates are considered. In practice, memory limitations usually require keeping m small.

6. Numerical experiments. We will investigate the behavior of the iteration and the influence of the different subspaces for the residual minimization discussed in [Section 5](#) by means of a checkerboard test problem [\[6\]](#). Here, the spatial domain is given by $R = (0, 7) \times (0, 7)$, the inflow boundary condition is given by $q_{\partial} = 0$, and the internal source term q as well as the scattering and absorption parameter, σ_s and σ_a , respectively, are defined in [Figure 6.1](#). Hence, the theoretical rate of [Theorem 1.2](#) is given by $\rho = \|\sigma_s/\sigma_t\|_{\infty} = 0.999$ here. We consider the Henyey-Greenstein scattering phase-function with anisotropy factor $0 \leq g < 1$, i.e.,

$$\theta(\mathbf{s} \cdot \mathbf{s}') := \frac{1}{4\pi} \frac{1 - g^2}{[1 - 2g(\mathbf{s} \cdot \mathbf{s}') + g^2]^{3/2}}.$$

If not stated otherwise, the domain R is triangulated using 100 352 elements, i.e., $n_R^+ = 50\,625$ and $n_R^- = 100\,352$. Moreover, we will employ 1024 elements on the half sphere, i.e., $n_S^+ = 1024$ and $n_S^- = 3072$, which results in 360 121 344 degrees of freedom. Spherical integration is performed by using a high-order numerical quadrature. We note that the accurate assembly of Θ^+ and Θ^- may require modified integration rules for $g = 0.99$. We chose to show results for this value of g to verify the robustness of our approach. For a sketch of a corresponding polyhedral approximation of the sphere see [Figure 6.1](#). We ran our code on a dual AMD EPYC 7742 64-Core Processor, i.e., 128 physical cores, with 1024 GB memory and Matlab R2023b with 128 workers. The code is freely available at [\[5\]](#). The iterations are stopped as soon as $\|\mathcal{R}_h(u_k)\|_{\sigma_t} < 10^{-6}$.

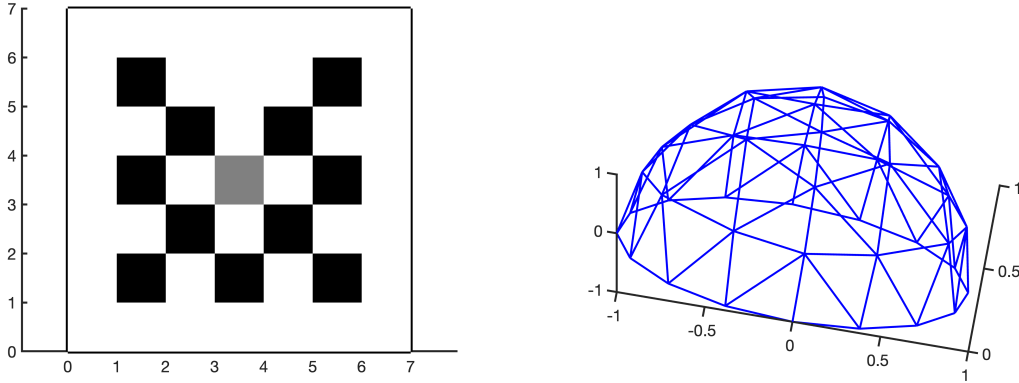


FIGURE 6.1. Left: geometry of the lattice problem in the checkerboard domain. White and gray areas are characterized by the optical parameters $\sigma_s = 10$ and $\sigma_a = 0.01$, while in the black zones $\sigma_s = 0$ and $\sigma_a = 1$. The internal source of radiation is $q = 1$ in the gray square, $q = 0$ outside of it. Right: Sketch of the spherical grid for the upper half sphere.

6.1. Minimization over $W_{h,N}^c$. We investigate the performance of the residual minimization strategy when using the subspace $W_{h,N}^c$ defined in [\(5.14\)](#) for different anisotropy parameters g . Furthermore, we investigate the behavior on the parameter K in [\(5.11\)](#). Here, we choose $K = 1, 6, 15$ such that it corresponds to the number of even spherical harmonics of degree at most $l = 0, 2, 4$, respectively. This choice is motivated by the observation that the $2l + 1$ spherical harmonics of degree l are eigenfunctions of Θ with eigenvalue g^l . For comparison, we also run the plain source iteration, cf. [\(1.3\)](#), which corresponds to the choice $K = 0$ and $W_{h,N} = \{0\}$, respectively.

The resulting numbers of iterations are displayed in Table 6.1. We observe that the required number of iterations are considerably smaller if residual minimization is performed, i.e., comparing the cases $K > 0$ and $K = 0$. As can also be seen from the decay of the residuals depicted in Figure 6.2, the minimization-based approach reduces the residual much faster than ρ^k with theoretical rate $\rho = 0.999$. We note that also the plain source iteration, $K = 0$, reduces the residual monotonically and slightly faster than predicted by theory, which might be explained by discretization effects, see also Table 6.3 (left), and the finite diameter of the domain \mathcal{R} [13]. Increasing K yields smaller iteration counts. In view of the computational complexity considerations made in Remark 5.3, the subspace correction computed here requires fewer floating point operations if the contraction rate of the residuals is better than $\rho^2 = 0.998$, because $\dim(W_{h,N}^c) = 1$ for $K > 0$. This is the case for all our experiments, as it is shown by the numbers in brackets in Table 6.1, indicating the maximum observed contraction rate $\max_k \|\mathcal{R}_h(u_k)\|_{\sigma_t} / \|\mathcal{R}_h(u_{k-1})\|_{\sigma_t}$ during the corresponding iterations.

TABLE 6.1

Iteration counts for minimization over $W_{h,N}^c$, defined in (5.14), for different anisotropy parameters g and order K of subspace correction, cf. (5.11). Observe that $K = 0$ corresponds to the source iteration without subspace correction, cf. (1.3). In brackets, $\max_k \|\mathcal{R}_h(u_k)\|_{\sigma_t} / \|\mathcal{R}_h(u_{k-1})\|_{\sigma_t}$.

| K | g | | | | | |
|-----|--------------|-------------|-------------|-------------|-------------|-------------|
| | 0.1 | 0.3 | 0.5 | 0.7 | 0.9 | 0.99 |
| 0 | 1018 (0.990) | 863 (0.988) | 701 (0.984) | 531 (0.979) | 358 (0.967) | 821 (0.989) |
| 1 | 62 (0.817) | 58 (0.805) | 54 (0.795) | 57 (0.809) | 97 (0.882) | 455 (0.981) |
| 6 | 20 (0.532) | 25 (0.603) | 14 (0.377) | 13 (0.371) | 31 (0.706) | 283 (0.973) |
| 15 | 12 (0.312) | 10 (0.245) | 8 (0.157) | 8 (0.216) | 18 (0.657) | 234 (0.969) |

TABLE 6.2

Average times (in seconds) per iteration for minimization over $W_{h,N}^c$, defined in (5.14), for different anisotropy parameters g and order K of subspace correction, cf. (5.11), with $K = 0$ the source iteration without subspace correction. In brackets, total time (in hours) taken by the iterative procedure.

| K | g | | | | | |
|-----|----------------|----------------|----------------|----------------|----------------|-----------------|
| | 0.1 | 0.3 | 0.5 | 0.7 | 0.9 | 0.99 |
| 0 | 66 s (18.72 h) | 66 s (15.93 h) | 68 s (13.32 h) | 67 s (9.98 h) | 66 s (6.63 h) | 69 s (15.87 h) |
| 1 | 156 s (2.70 h) | 153 s (2.48 h) | 153 s (2.30 h) | 155 s (2.46 h) | 153 s (4.14 h) | 155 s (19.59 h) |
| 6 | 151 s (0.84 h) | 158 s (1.10 h) | 157 s (0.61 h) | 159 s (0.57 h) | 156 s (1.35 h) | 160 s (12.65 h) |
| 15 | 163 s (0.54 h) | 168 s (0.47 h) | 170 s (0.38 h) | 168 s (0.37 h) | 164 s (0.82 h) | 167 s (10.86 h) |

As discussed in Remark 5.3 each iteration of the residual minimization scheme requires more operations than the source iteration. Therefore, we also compare the runtime of these methods using our implementation. In order to solve the linear systems in (5.10) and (5.13) we use sparse LU-factorizations, which are precomputed before entering the iteration. For finer discretizations than the ones we use here, such a pre-computation might be restrictive in terms of memory. To solve (5.13) more efficiently for larger systems, we refer to [11] for a conjugate gradient method with a multigrid preconditioner. In any case, improved solvers for (5.10) are equally beneficial for

both the usual source iteration as well as the residual minimization based approach. In Table 6.2 we display the average runtime per step as well as the overall runtime for the considered methods. These timings match the theoretical considerations of Remark 5.3. Moreover, the computation time required for computing the solution to (5.13), has a runtime less than one solve of (5.10), which can be seen from comparing the rows for $K > 0$ with the row $K = 0$. Because of these observations, we do not show further timings but use computational complexity considerations to discuss the different methods in the following numerical experiments.

TABLE 6.3

Iteration counts for minimization over $W_{h,N}^c$, defined in (5.14), for $g = 0.7$ and $K = 0$ (left) and $K = 6$ (right), and different spatial and angular grids.

| $K = 0$ | | | | | $K = 6$ | | | | |
|---------|---------|-----|-----|------|---------|---------|----|-----|------|
| n_R^+ | n_S^+ | | | | n_R^+ | n_S^+ | | | |
| | 16 | 64 | 256 | 1024 | | 16 | 64 | 256 | 1024 |
| 841 | 475 | 483 | 487 | 488 | 841 | 8 | 8 | 9 | 9 |
| 3 249 | 499 | 509 | 514 | 515 | 3 249 | 8 | 9 | 10 | 10 |
| 12 769 | 509 | 520 | 525 | 526 | 12 769 | 8 | 10 | 11 | 11 |
| 50 625 | 513 | 524 | 529 | 531 | 50 625 | 9 | 11 | 12 | 13 |

Before testing the performance of the approach on the next subspace for minimization, let us discuss Table 6.3, where we show the iteration counts for the choices $g = 0.7$ and $K = 0$ (left) and $K = 6$ (right), and for different angular and spatial grids obtained by successive refinements. We observe that the number of iterations varies only slightly upon mesh refinement, which we expect because we derived the iteration from its infinite-dimensional counterpart.

6.2. Minimization over $\tilde{W}_{h,N}^c$. As a second test case, we study how the residual minimization approach performs over the enriched subspace $\tilde{W}_{h,N}^c$ defined in (5.15). Since the source iteration (1.3) does not depend on the chosen subspace, the reader may refer to the $K = 0$ row in Table 6.1 for corresponding iteration numbers. As can be seen from Table 6.4, for moderate values of the anisotropy factor g the improvement in the number of iterations is negligible with respect to minimization over $W_{h,N}^c$. However, for highly forward-peaked scattering, $g = 0.99$, which causes the iteration to be notably slower than the other cases, the improvement is more visible, even for low order corrections ($K = 1$). Figure 6.3 shows the convergence history of the residuals, and we observe a robust convergence behavior. Since $\dim(\tilde{W}_{h,N}^c) = 4$, minimization over this subspace is useful in terms of the theoretical computational complexity considerations if the contraction rate of the residuals stays below $\rho^5 = 0.995$, cf. Remark 5.3. Once again, our method achieves this requirement, as shown in brackets in Table 6.4. Except for $g \in \{0.9, 0.99\}$ and $K = 1$, we also have that $(\rho_{SI}^g)^5 > \max_k \|\mathcal{R}_h(u_k)\|_{\sigma_t} / \|\mathcal{R}_h(u_{k-1})\|_{\sigma_t}$ with ρ_{SI}^g denoting the observed (worst) contraction rate of the source iteration as displayed in Table 6.1, i.e., minimization over $\tilde{W}_{h,N}^c$ is more efficient.

6.3. Minimization over $\tilde{W}_{h,N}^{c,m}$. Exploiting Anderson-type acceleration techniques as described in Subsection 5.4.3 we observe a substantial reduction in the iteration count for all values of g and already for moderate m and low-order corrections. Indeed, comparing Table 6.4 and Table 6.5, where a history of $m = 2$ iterates is taken into account for residual minimization and thus $\dim(\tilde{W}_{h,N}^{c,2}) = 6$, we notice that already for $K = 1$ the number of iterations is roughly reduced by a factor of 3 for small g and a factor of 2 for g close to 1. The numbers in Table 6.6, where $m = 4$

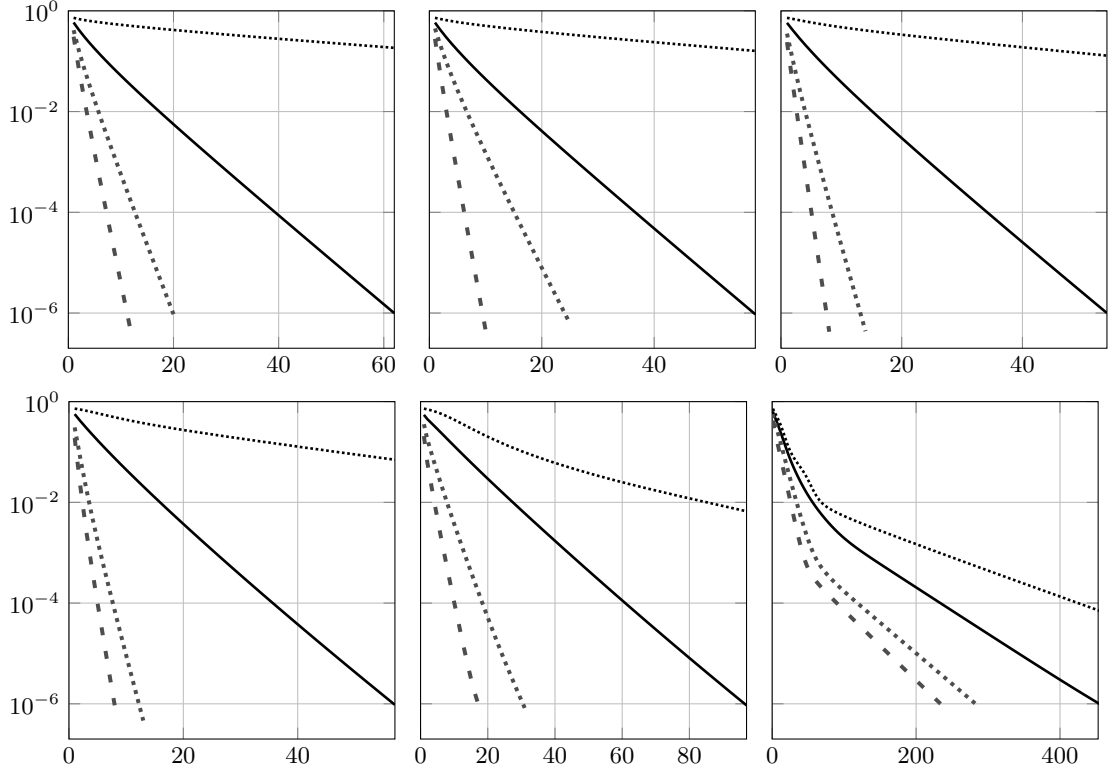


FIGURE 6.2. Residual decay for correction searched in the subspace $W_{h,N}^c$. From left to right, we plot $\|\mathcal{R}_h(u_k)\|_{\sigma_t}$; first row $g = 0.1, 0.3, 0.5$; second row, $g = 0.7, 0.9, 0.99$. The lines' style refers to number of even eigenfunctions of the scattering operator employed: $K = 0$ (standard source iteration) densely dotted line; $K = 1$ solid line; $K = 6$ dotted line; $K = 15$ dashed line.

TABLE 6.4
Iteration counts for minimization over $\tilde{W}_{h,N}^c$ defined in (5.15) for different anisotropy parameters g and order K of subspace correction, cf. (5.11). In brackets $\max_k \|\mathcal{R}_h(u_k)\|_{\sigma_t} / \|\mathcal{R}_h(u_{k-1})\|_{\sigma_t}$.

| K | g | | | | | |
|-----|------------|------------|------------|------------|------------|-------------|
| | 0.1 | 0.3 | 0.5 | 0.7 | 0.9 | 0.99 |
| 1 | 58 (0.804) | 54 (0.792) | 51 (0.785) | 56 (0.807) | 98 (0.893) | 388 (0.975) |
| 6 | 18 (0.487) | 22 (0.571) | 12 (0.324) | 13 (0.371) | 26 (0.621) | 123 (0.940) |
| 15 | 11 (0.284) | 9 (0.219) | 8 (0.142) | 8 (0.213) | 16 (0.449) | 93 (0.879) |

was chosen, are comparable to those in Table 6.5. Thus, we prefer the choice $m = 2$ because it requires less memory. The computational complexity does not increase with m in practice because the residuals of the previous iterates can be stored in memory. Therefore, although $N = 6$ and $N = 8$ for $m = 2$ and $m = 4$, respectively, the number of residual computations is as in the previous subsection, i.e., 5 per step. Since for $g < 0.99$ or $K > 1$ both ρ^5 as well as $(\rho_{SI}^g)^5$ are larger

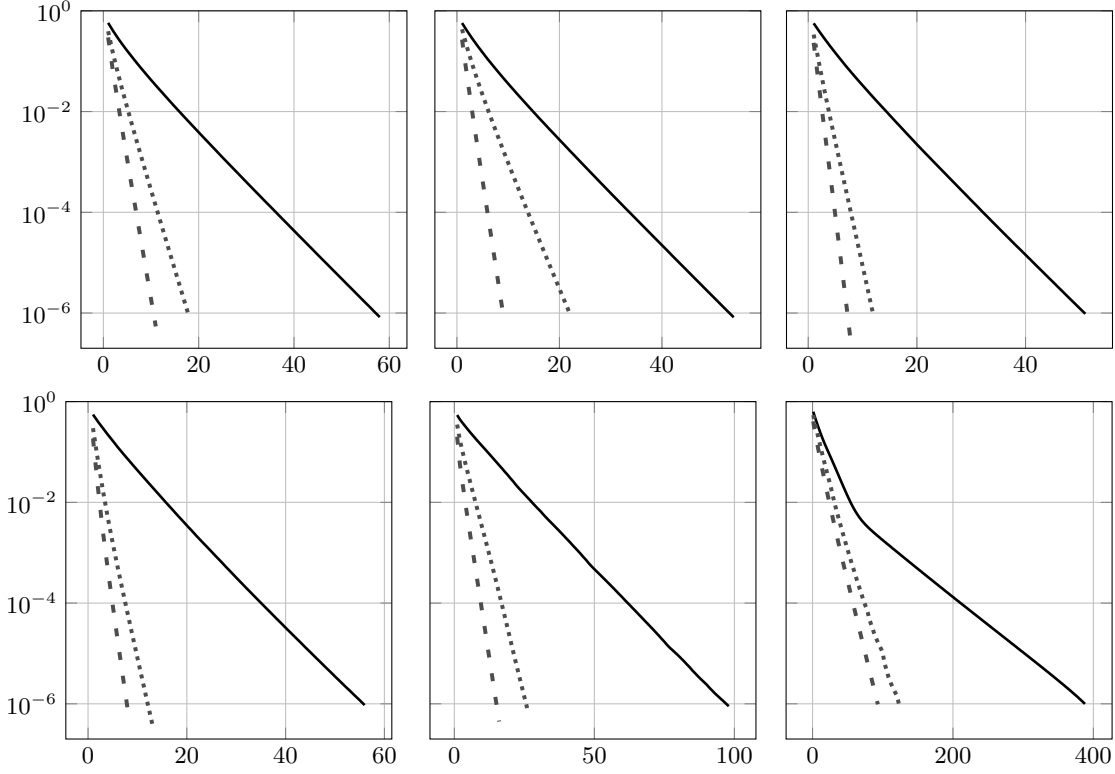


FIGURE 6.3. Residual decay for correction searched in the subspace $\tilde{W}_{h,N}^c$. From left to right, we plot $\|\mathcal{R}_h(u_k)\|_{\sigma_t}$; first row $g = 0.1, 0.3, 0.5$; second row, $g = 0.7, 0.9, 0.99$. The lines style refers to the dimension of the corrections subspace: $K = 1$ solid line; $K = 6$ dotted line; $K = 15$ dashed line.

than the observed contraction rates as shown in brackets in Table 6.5 and Table 6.6, the proposed methodology is more efficient than the source iteration.

TABLE 6.5
Iteration counts for minimization over $\tilde{W}_{h,N}^{c,2}$ defined in (5.16) for different anisotropy parameters g and order K of subspace correction, cf. (5.11). In brackets $\max_k \|\mathcal{R}_h(u_k)\|_{\sigma_t} / \|\mathcal{R}_h(u_{k-1})\|_{\sigma_t}$.

| $m = 2$ | g | | | | | |
|---------|------------|------------|------------|------------|------------|-------------|
| K | 0.1 | 0.3 | 0.5 | 0.7 | 0.9 | 0.99 |
| 1 | 17 (0.500) | 17 (0.483) | 20 (0.579) | 27 (0.667) | 42 (0.778) | 262 (0.975) |
| 6 | 9 (0.224) | 10 (0.237) | 8 (0.172) | 9 (0.210) | 19 (0.518) | 96 (0.937) |
| 15 | 7 (0.119) | 7 (0.100) | 6 (0.076) | 7 (0.121) | 13 (0.375) | 67 (0.838) |

7. Conclusions and discussion. In this paper, we have developed a generic and flexible strategy to accelerate the source iteration for the solution of anisotropic radiative transfer problems using residual minimization. We showed convergence of the resulting method for any choice of

TABLE 6.6
Iteration counts for minimization over $\tilde{W}_{h,N}^{c,4}$ defined in (5.16) for different anisotropy parameters g and order K of subspace correction, cf. (5.11). In brackets $\max_k \|\mathcal{R}_h(u_k)\|_{\sigma_t} / \|\mathcal{R}_h(u_{k-1})\|_{\sigma_t}$.

| $m = 4$ | g | | | | | |
|---------|------------|------------|------------|------------|------------|-------------|
| K | 0.1 | 0.3 | 0.5 | 0.7 | 0.9 | 0.99 |
| 1 | 16 (0.671) | 17 (0.675) | 17 (0.689) | 22 (0.721) | 39 (0.810) | 218 (0.968) |
| 6 | 11 (0.598) | 13 (0.751) | 10 (0.324) | 11 (0.540) | 19 (0.569) | 92 (0.918) |
| 15 | 9 (0.606) | 10 (0.685) | 9 (0.527) | 8 (0.492) | 13 (0.446) | 63 (0.847) |

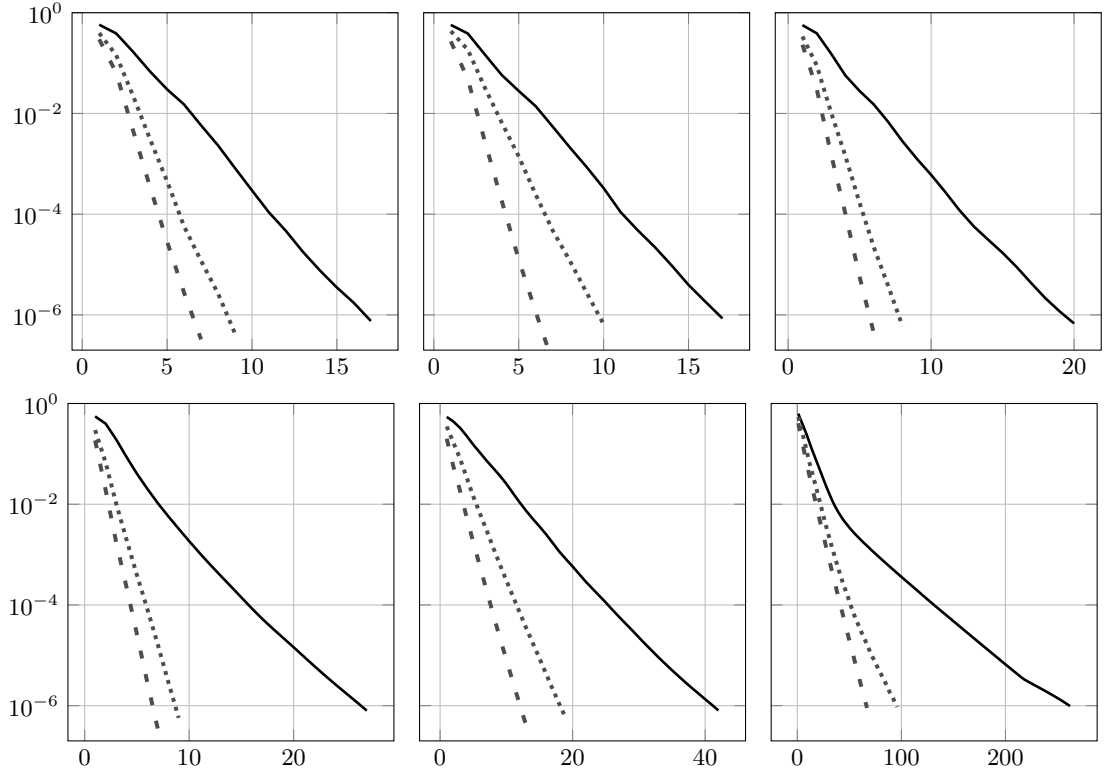


FIGURE 6.4. Residual decay for correction searched in the subspace $\tilde{W}_{h,N}^{c,2}$. From left to right, we plot $\|\mathcal{R}_h(u_k)\|_{\sigma_t}$; first row $g = 0.1, 0.3, 0.5$; second row, $g = 0.7, 0.9, 0.99$. The lines' style refers to number of even eigenfunctions of the scattering operator employed: $K = 1$ solid line; $K = 6$ dotted line; $K = 15$ dashed line.

subspace employed in the residual minimization. The flexibility in choosing the subspace was used to exploit high-order diffusion corrections, which were shown to be effective for highly forward-peaked scattering. Moreover, the numerical results confirmed that the required iteration counts do depend on the discretization only mildly.

We mention that our approach can be seen as a two-level scheme. We leave it to future work to extend it and compare it to angular multilevel schemes. Moreover, the analysis of the precise

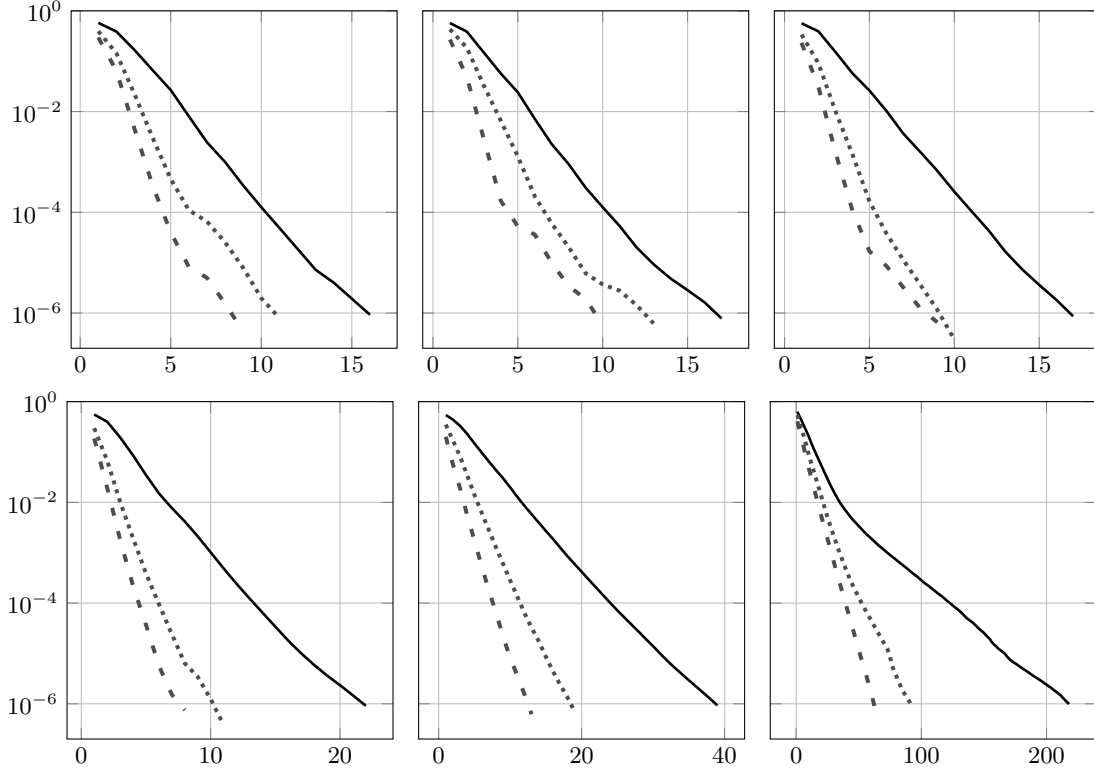


FIGURE 6.5. Residual decay for correction searched in the subspace $\tilde{W}_{h,N}^{c,4}$. From left to right, we plot $\|\mathcal{R}_h(u_k)\|_{\sigma_t}$; first row $g = 0.1, 0.3, 0.5$; second row, $g = 0.7, 0.9, 0.99$. The lines' style refers to number of even eigenfunctions of the scattering operator employed: $K = 1$ solid line; $K = 6$ dotted line; $K = 15$ dashed line.

approximation properties of the considered subspaces is also left to future research. We close by mentioning that the efficient and robust solution of the source problem (1.1) is also relevant for solving eigenvalue problems, see, e.g., [4, 7, 27].

Acknowledgements. R.B. and M.S. acknowledge support by the Dutch Research Council (NWO) via grant OCENW.KLEIN.183.

REFERENCES

- [1] M. L. ADAMS AND E. W. LARSEN, *Fast iterative methods for discrete-ordinates particle transport calculations*, Prog. Nuclear Energy, 40 (2002), pp. 3–159, [https://doi.org/10.1016/S0149-1970\(01\)00023-3](https://doi.org/10.1016/S0149-1970(01)00023-3).
- [2] D. Y. ANISTRATOV AND J. S. WARSA, *Discontinuous finite element quasi-diffusion methods*, Nucl. Sci. Eng., 191 (2018), pp. 105–120, <https://doi.org/10.1080/00295639.2018.1450013>.
- [3] S. R. ARRIDGE AND J. C. SCHOTLAND, *Optical tomography: forward and inverse problems*, Inverse Problems, 25 (2009), pp. 123010, 59, <https://doi.org/10.1088/0266-5611/25/12/123010>.
- [4] A. P. BARBU AND M. L. ADAMS, *Convergence properties of a linear diffusion-acceleration method for k -eigenvalue transport problems*, Nucl. Sci. Eng., 197 (2022), pp. 517–533, <https://doi.org/10.1080/00295639.2022.2123205>.
- [5] R. BARDIN AND M. SCHLOTTBOM, *Code underlying the publication: On accelerated iterative schemes for*

- anisotropic radiative transfer using residual minimization, <https://doi.org/10.5281/zenodo.14750632>.
- [6] T. A. BRUNNER, *Forms of approximate radiation transport*, in Nuclear Mathematical and Computational Sciences: A Century in Review, A Century Anew Gatlinburg, LaGrange Park, IL, 2003, American Nuclear Society. Tennessee. April 6–11, 2003.
 - [7] M. T. CALEF, E. D. FICHTL, J. S. WARSA, M. BERNDT, AND N. N. CARLSON, *Nonlinear Krylov acceleration applied to a discrete ordinates formulation of the k -eigenvalue problem*, J. Comput. Phys., 238 (2013), pp. 188–209, <https://doi.org/https://doi.org/10.1016/j.jcp.2012.12.024>.
 - [8] K. M. CASE AND P. F. ZWEIFEL, *Existence and uniqueness theorems for the neutron transport equation*, J. Math. Phys., 4 (1963), pp. 1376–1385, <https://doi.org/10.1063/1.1703916>.
 - [9] K. M. CASE AND P. F. ZWEIFEL, *Linear transport theory*, Addison-Wesley Publishing Co., Reading, Mass.-London-Don Mills, Ont., 1967.
 - [10] S. DARGAVILLE, A. BUCHAN, R. SMEDLEY-STEVENSON, P. SMITH, AND C. PAIN, *A comparison of element agglomeration algorithms for unstructured geometric multigrid*, J. Comput. Appl. Math., 390 (2021), p. 113379, <https://doi.org/https://doi.org/10.1016/j.cam.2020.113379>.
 - [11] J. DÖLZ, O. PALII, AND M. SCHLOTTBOM, *On robustly convergent and efficient iterative methods for anisotropic radiative transfer*, J. Sci. Comput., 90 (2022), <https://doi.org/10.1007/s10915-021-01757-9>.
 - [12] H. EGGER AND M. SCHLOTTBOM, *A mixed variational framework for the radiative transfer equation*, Math. Models Methods Appl. Sci., 22 (2012), pp. 1150014, 30, <https://doi.org/10.1142/S021820251150014X>.
 - [13] H. EGGER AND M. SCHLOTTBOM, *An L_p theory for stationary radiative transfer*, Appl. Anal., 93 (2013), pp. 1283–1296, <https://doi.org/10.1080/00036811.2013.826798>.
 - [14] K. F. EVANS, *The spherical harmonics discrete ordinate method for three-dimensional atmospheric radiative transfer*, J. Atmospheric Sci., 55 (1998), pp. 429–446, [https://doi.org/10.1175/1520-0469\(1998\)055<0429:TSHDOM>2.0.CO;2](https://doi.org/10.1175/1520-0469(1998)055<0429:TSHDOM>2.0.CO;2).
 - [15] T. S. HAUT, B. S. SOUTHWORTH, P. G. MAGINOT, AND V. Z. TOMOV, *Diffusion synthetic acceleration preconditioning for discontinuous Galerkin discretizations of S_N transport on high-order curved meshes*, SIAM J. Sci. Comput., 42 (2020), pp. B1271–B1301, <https://doi.org/10.1137/19M124993X>.
 - [16] H. HENSEL, R. IZA-TERAN, AND N. SIEDOW, *Deterministic model for dose calculation in photon radiotherapy*, Phys. Med. Biol., 51 (2006), pp. 675–693, <https://doi.org/10.1088/0031-9155/51/3/013>.
 - [17] G. KANSCHAT AND J.-C. RAGUSA, *A robust multigrid preconditioner for S_N -DG approximation of monochromatic, isotropic radiation transport problems*, SIAM J. Sci. Comput., 36 (2014), pp. A2326–A2345, <https://doi.org/10.1137/13091600x>, <http://dx.doi.org/10.1137/13091600X>.
 - [18] B. LEE, *A novel multigrid method for S_n discretizations of the mono-energetic Boltzmann transport equation in the optically thick and thin regimes with anisotropic scattering, part I*, SIAM J. Sci. Comput., 31 (2010), pp. 4744–4773, <https://doi.org/10.1137/080721480>, <http://dx.doi.org/10.1137/080721480>.
 - [19] G. I. MARCHUK AND V. I. LEBEDEV, *Numerical methods in the theory of neutron transport*, Harwood Academic Publishers, Chur, second ed., 1986.
 - [20] X. MENG, S. WANG, G. TANG, J. LI, AND C. SUN, *Stochastic parameter estimation of heterogeneity from crosswell seismic data based on the Monte Carlo radiative transfer theory*, J. Geophys. Eng., 14 (2017), pp. 621–633, <https://doi.org/10.1088/1742-2140/aa6130>.
 - [21] S. OLIVIER, W. PAZNER, T. S. HAUT, AND B. C. YEE, *A family of independent variable eddington factor methods with efficient preconditioned iterative solvers*, J. Comput. Phys., 473 (2023), p. 111747, <https://doi.org/https://doi.org/10.1016/j.jcp.2022.111747>.
 - [22] O. PALII AND M. SCHLOTTBOM, *On a convergent DSA preconditioned source iteration for a DGFEM method for radiative transfer*, Comput. Math. Appl., 79 (2020), pp. 3366–3377, <https://doi.org/10.1016/j.camwa.2020.02.002>.
 - [23] J. RAGUSA, J.-L. GUERMOND, AND G. KANSCHAT, *A robust S_N -DG-approximation for radiation transport in optically thick and diffusive regimes*, J. Comput. Phys., 231 (2012), pp. 1947–1962, <https://doi.org/https://doi.org/10.1016/j.jcp.2011.11.017>.
 - [24] J. C. RAGUSA AND Y. WANG, *A two-mesh adaptive mesh refinement technique for S_N neutral-particle transport using a higher-order DGFEM*, J. Comput. Appl. Math., 233 (2010), pp. 3178–3188, <https://doi.org/10.1016/j.cam.2009.12.020>.
 - [25] T. P. ROBITAILLE, *Hyperion: an open-source parallelized three-dimensional dust continuum radiative transfer code*, A&A, 536 (2011), p. A79, <https://doi.org/10.1051/0004-6361/201117150>.
 - [26] M. RUSTAMZHON, D. PRESS, G. K. BASKARAN, S. SADEGHI, AND S. NIZAMOGLU, *Unravelling radiative energy transfer in solid-state lighting*, J. Appl. Phys., 123 (2018), <https://doi.org/10.1063/1.5008922>.
 - [27] Q. SHEN AND B. KOCHUNAS, *Practical considerations for the adoption of Anderson acceleration in nonlinear diffusion accelerated transport*, Ann. Nucl. Energy, 199 (2024), p. 110330, <https://doi.org/10.1016/j.anucene.2023.110330>.

- [28] Q. SHENG AND C. D. HAUCK, *Uniform convergence of an upwind discontinuous Galerkin method for solving scaled discrete-ordinate radiative transfer equations with isotropic scattering*, Math. Comp., 90 (2021), pp. 2645–2669, <https://doi.org/10.1090/mcom/3670>.
- [29] B. S. SOUTHWORTH, M. HOLEC, AND T. S. HAUT, *Diffusion synthetic acceleration for heterogeneous domains, compatible with voids*, Nucl. Sci. Eng., 195 (2020), pp. 119–136, <https://doi.org/10.1080/00295639.2020.1799603>.
- [30] K. STAMNES, G. THOMAS, AND J. STAMNES, *Radiative transfer in the atmosphere and ocean*, Modeling and Simulation in Science, Engineering and Technology, Cambridge University Press, 2nd ed., 2017, <https://doi.org/10.1017/9781316148549>.
- [31] Z. SUN AND C. D. HAUCK, *Low-memory, discrete ordinates, discontinuous Galerkin methods for radiative transport*, SIAM J. Sci. Comput., 42 (2020), pp. B869–B893, <https://doi.org/10.1137/19M1271956>, <https://doi.org/10.1137/19M1271956>.
- [32] B. TURCKIN, J. C. RAGUSA, AND J. E. MOREL, *Angular multigrid preconditioner for Krylov-based solution techniques applied to the S_N equations with highly forward-peaked scattering*, Transport Theor. Stat., 41 (2012), pp. 1–22, <https://doi.org/10.1080/00411450.2012.672944>.
- [33] H. F. WALKER AND P. NI, *Anderson acceleration for fixed-point iterations*, SIAM J. Numer. Anal., 49 (2011), pp. 1715–1735, <https://doi.org/10.1137/10078356X>.
- [34] J. S. WARSA AND D. Y. ANISTRATOV, *Two-level transport methods with independent discretization*, J. Comput. Theor. Transp., 47 (2018), pp. 424–450, <https://doi.org/10.1080/23324309.2018.1497991>.
- [35] J. S. WARSA, T. A. WAREING, AND J. E. MOREL, *Krylov iterative methods and the degraded effectiveness of diffusion synthetic acceleration for multidimensional S_N calculations in problems with material discontinuities*, Nucl. Sci. Eng., 147 (2004), pp. 218–248, <https://doi.org/10.13182/nse02-14>.
- [36] J. WILLERT, H. PARK, AND W. TAITANO, *Using Anderson acceleration to accelerate the convergence of neutron transport calculations with anisotropic scattering*, Nucl. Sci. Eng., 181 (2015), pp. 342–350, <https://doi.org/10.13182/nse15-16>.